IEEE Access
Multidisciplinary | Rapid Review | Open Access Journal

IEEE POWER & ENERGY SOCIETY SECTION

Received 12 June 2023, accepted 13 July 2023, date of publication 17 July 2023, date of current version 28 July 2023.

Digital Object Identifier 10.1109/ACCESS.2023.3296220

RESEARCH ARTICLE

Grid Impact of Frequency Regulation Provided by V2Gs Aggregated at HV, MV, and LV Level

MARTA BERNAL-SANCHO[1], ROBERTO ROCCA[1,2], (Member, IEEE), GREGORIO FERNÁNDEZ-AZNAR[1], MARÍA PAZ COMECH[2], AND NOEMÍ GALÁN-HERNÁNDEZ[1]

[1]Electrical Systems Department, CIRCE Technology Centre, 50018 Zaragoza, Spain
[2]CIRCE Technology Centre, CIRCE Mixed Research Institute, University of Zaragoza, 50018 Zaragoza, Spain

Corresponding author: Marta Bernal-Sancho (mbernal@fcirce.es)

This work was supported by the European Union's Horizon 2020 Research and Innovation Program Developed within the Framework of the 'Large demonstratIoN of user CentrIc urban and longrange charging solutions to boosT an engaging deployment of Electric Vehicles in Europe' — 'INCIT-EV' Project under Grant 875683.

ABSTRACT Vehicle-to-Grid chargers (V2Gs) are currently considered a key component for supporting future power systems in primary and especially secondary frequency regulation. Most of the research works conducted so far on this topic are based on a vehicle-centric perspective, whereas global approaches where the impact caused by fleets of V2Gs is studied from the perspective of an entire electric grid remain quite unexplored. In particular, the effects of aggregating different amounts of V2Gs from the HV, MV and LV subgrids to participate in frequency control represents a novel aspect to be investigated, which is expected to possess a strong potential for further improving the aggregation processes. To this end, this work presents a ''global working framework'' developed to evaluate the impact on an entire electric system of V2Gs participation in frequency regulation. A reality-based electric network is considered, where two HV, three MV and ten LV subgrids are interconnected. The effects of four different percentages of V2Gs aggregated from the HV, MV and LV subgrids are evaluated for two V2G installed capacities, 10 MW and 20 MW. Results are finally analyzed, including frequency vs time response, rate of change of frequency, grid losses, etc., and valuable knowledge, insights and guidelines are obtained for guiding future grid-level aggregation optimizations of V2Gs participation in frequency regulation.

INDEX TERMS Impact, evaluation, frequency regulation, frequency control, electric vehicle, vehicle-to-grid, ancillary services, overfrequency, underfrequency, state of charge, aggregator, voltage levels.

I. INTRODUCTION

The environmental goals that almost all the world's leading countries are pursuing to meet the 2030 - 2050 CO_2 emission limits require the installation of several TWs of renewable energy sources. Their integration, in turn, demands enormous investments in advanced and distributed energy storage systems [1], [2].

Another aspect to highlight is the massive electrification of transportation systems [3], [4]. Consequently, from the last decade, plug-in-hybrid and full Electric Vehicles (EVs) are experiencing an accelerated deployment, which is fostered by the steady cost reduction in both electric powertrains and battery packs [5]. Extensive studies are currently underway to optimize their integration with renewable-based and virtual power plants [6], [7].

Together with the onboard systems, the charging infrastructure stands as an additional essential element for transportation electrification. Indeed, charging infrastructure is evolving very fast, and one of the main challenges is currently the transition from the old-fashion unidirectional chargers to bidirectional chargers, referred to as Vehicle-to-Grid (V2G) [8].

The V2G technology allows a two-way energy flow between EVs battery packs and the grid, which, in turn, opens new possible interactions between them. In fact, according to [9], cars travel for approximately only 5% of the day, remaining unused the rest of the time. Consequently, fleets of unused, plugged-in EVs possess a huge potential for supporting future grids in different ways [3], such as

The associate editor coordinating the review of this manuscript and approving it for publication was Peter Palensky.

distributed battery storage systems [10], provision of virtual inertia [11], or frequency control [12], provided that V2Gs are appropriately aggregated.

Concerning frequency control services, literature works span many different aspects. Firstly, the design, analysis and modelling of aggregation algorithms are tackled. Reference [13] investigates the effects of communication time delay on the system stability in single-area frequency control, whilst [14] proposes deep and reinforcement learning methods to model the EV uncertainties and their heterogeneous States of Charge (SoC) to optimize the aggregation process. Secondly, different constraints to the EVs' participation in frequency support are analyzed, such as the maintenance of a minimum SoC [15] or battery degradation [16], or even with multi-objective functions that include: minimization of frequency deviations at the grid level; users preferences; reduction of battery degradation and users revenues maximization [17]. Other key factors widely analyzed in the literature are market participation and remuneration schemes. Here, some research works deal with the optimization of regulation capacity bids [18], milage payment for aggregators to compensate for response delays [19] or charging scheduling optimization [20]. At this point, the key point to note is that compensation mechanisms for EV owners need to consider that market utilities normally remunerate the participation in frequency control for both capacity provision and activation upon request [21], [22], [23]. Besides, business models have been proposed to remunerate battery degradation [24]. Finally, other trending topics are the V2G support in frequency control of microgrids [25], [26], along with the participation of V2G fleets in demand-side management mechanisms [27].

From the analysis above, the key points that emerge are as follows:

1. All contributions are based on a vehicle-centric approach, whereas grid-level approaches are much less mature.
2. Most proposed aggregation processes focus on SoC constraints, optimal forecasting, scheduling, etc. By contrast, little or no attention is paid to the benefits of aggregating EVs from different voltage levels of the same grid.

Regarding point 1, few grid-level studies and analyses have been published. Here, the main focus is on using EV fleets as an alternative to static storage solutions for integrating renewable energy generation rather than deep grid-level analyses [28], [29]. Concerning point 2, as already mentioned above, the main stochastic elements taken into account for the aggregation processes are the EVs SoC distribution, available power capacity, EV number, etc. [15], [16], [17], [18], [19], [20]. On the other hand, effects of aggregating different EV amounts at HV, MV and LV subgrids are not considered. Finally, it is worth noting that most contributions above consider benchmark and library grids, so that experience from the real world using reality-based grids and data could be of great help for guiding future research works.

To fill the bespoke gaps in the state of the art, this paper proposes the analysis of the impact of V2G participation in frequency regulation using a grid-centric model. The analyzed network consists of two HV transmission subgrids, three MV subtransmission subgrids and ten LV distribution subgrids. A 10 MW and a 20 MW V2Gs global capacity are distributed in different proportions among the HV, MV and LV levels. In particular, in the case of the HV, the idea is to represent near-future situations where V2G stations are located in ''fuel'' stations on highways, as well as chargers installed near HV/MV substations or V2G stations owned by industrial facilities connected through transformers and power lines with negligible length to the transmission network. Finally, a set of Key Performance Indicators (KPIs) are thoroughly compared and analyzed to obtain valuable knowledge, insights and guidelines for future grid-level optimization of V2G aggregation for frequency regulation. All of this constitutes a ''global working framework'' based on the electric system defined in the EU-H2020 project INCIT-EV [30].

To recap all the above, the main contributions this paper aims to provide are as follows:

- Study and analysis of EVs' participation in frequency events in a reality-based grid composed of HV, MV and LV subgrids.
- Assessment of the effects of aggregating different EV amounts at HV, MV and LV levels.
- Assessment via KPIs defined by taking the perspective of the grid into account.

This manuscript is structured as follows. Section II provides a brief technical background on frequency regulation with V2Gs. Section III describes the V2G and the frequency control models used in this work. Section IV summarizes the Key Performance Indicators (KPIs). Section V describes the ''global working framework,'' defining the grid topology, the V2G rated power and energy capacities, the frequency event, and the V2G installed capacities and aggregation scenarios. Finally, simulation results are shown and discussed in section VI.

II. FREQUENCY CONTROL AND V2G CHARGERS

Frequency control is responsible for regulating the amount of active power generated in response to a load variation so that frequency is kept within its permitted values, i.e., $f_0 \pm \Delta f$.

In particular, frequency adjustment measures are divided into three subcontrols, as illustrated in Figure 1 [31].

Primary control is a fast regulation that responds as soon as a frequency deviation exceeds the permitted value, aimed at minimizing both the transient frequency (frequency nadir, f_{nadir}) and the Rate of Change of Frequency ($RoCoF$). Secondary control is a slow-response regulation that intervenes after the primary. Its objective is to maintain frequency at a stable value f_{fin}, albeit outside the permitted range. Finally, tertiary control takes place after the secondary to restore frequency within its permitted values.

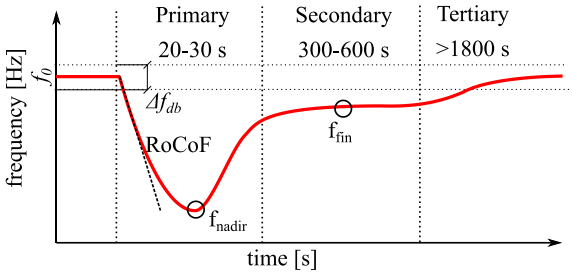

FIGURE 1. Typical system response to an underfrequency event [31].

Tertiary control is currently covered through high-inertia, high-capacity power plants, such as nuclear or coal-fired. In future grids, tertiary control is expected to be covered by long-term, high-capacity storage or demand response mechanisms [32]. Consequently, as widely confirmed by the literature [12], [33], it is reasonable to assume that V2G chargers participate only in primary and especially secondary frequency regulation.

In particular, the power and energy a V2G fleet can provide in primary and secondary regulation must follow the legislative and market mechanisms. As an example of a current EU scenario with a high penetration of renewables, this work considers the current Spanish situation [34], [35]. Nowadays, according to the Spanish TSO, support of the grid in the primary frequency regulation is mandatory but not remunerated, and primary regulation of the generating groups must ensure a statism level in their control that allows their output to vary by 1.5 percent of the rated power. On the other hand, secondary frequency regulation is remunerated for both capacity reserve and activation based on a market auction mechanism, which enhances EV fleets to provide this service [35].

III. V2G STATION MODEL

V2G stations have been modelled in this work as a Pulse-Width-Modulation (PWM) converter connected to a Battery Energy Storage System (BESS), as shown in Figure 2.

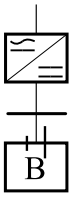

FIGURE 2. Schematic representation of a V2G charging station.

The complete control scheme comprises four main blocks, as represented in Figure 3 [36]. The *PQ Control* regulates both the V2G reactive and active power. Here, the Q control adjusts the AC voltage or the injected/absorbed reactive power, and its output is the q-axis current reference $i_{q\_ref\_in}$. On the other hand, the P Control regulates both DC-bus voltage and grid frequency, and its output is the d-axis current reference $i_{d\_ref\_in}$.

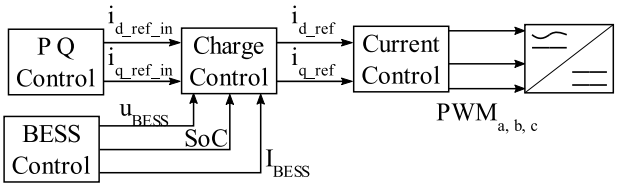

FIGURE 3. V2G controllers, blocking scheme [36].

In the *BESS Control*, the main parameters of the battery pack, such as the number of cells in series and parallel or cell capacity, are defined. As output, the state of charge (*SoC*), voltage and current of the BESS are given. Subsequently, the *Charge Control* receives signals from both *PQ control* and *BESS Control* and limits the absolute V2G current value always prioritizing the d- over the q-axis current; its output signals are i_{d_ref} and i_{q_ref}. Regarding the *PQ Control*, it is worth highlighting that in case of a frequency event, the control system acts to deliver/absorb all the active power available so that the Q control remains temporarily disabled. Finally, the *Current Control* includes proportional-integral controllers (PIs), which track the current setpoints set by the *Charge Control* and produce the voltage references for the PWM converter.

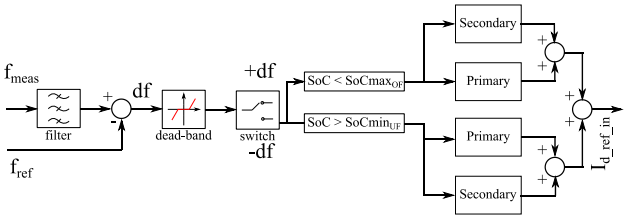

FIGURE 4. Primary and secondary frequency regulation controls.

Further into detail, the frequency control possesses both primary and secondary frequency regulation subcontrols, shown in Figure 4. In accordance with section II, the conditions defined by the Spanish TSO in [34] and [35] are considered to set the primary and secondary control parameters. Here, it is worth observing that two separate loops are introduced for under and overfrequency phenomena. Moreover, the initial *SoC* of the EVs is considered in frequency control since the final *SoC* after participation in a grid-support event is expected to be a critical factor in defining users' willingness to participate in frequency events. Consequently, SoC limitations have been included in the control system considering both the aggregation and the activation stages:

- In underfrequency events, a V2G must feed active power to the grid. Thus, in these events, an acceptable final *SoC* level must be ensured for all users. Therefore, it has been assumed that only EVs with an initial *SoC* higher than $SoCmin_{UF}$ can provide the frequency correction service. As V2Gs provide power to the grid and hence their *SoC* decreases, a minimum allowed *SoC* has been set to SoC_{min}, at which power delivery is interrupted. The idea

with this limit is to preserve a minimum level of stored energy for the EV owners, which must be sufficient to cover a typical driving cycle.

- In overfrequency events, V2Gs must work as loads consuming active power, although at a different intensity with respect to the value before the event. Thus, to be eligible to be aggregated for contribution to an overfrequency event, the initial *SoC* level of an EV must be lower than the limit $SoCmax_{OF}$. In fact, the influence of EVs with a high SoC is minimum as they would absorb power for a relatively short time. Then, power absorption is naturally interrupted as the *SoC* is 1.

In order to visualize some key features of the V2Gs during a frequency event, Figure 5 shows the behavior of one V2G station connected to a 0.4 kV distribution subgrid during an underfrequency event. The event occurs in the instant indicated by the dotted vertical line. In these tests, $SoCmin_{UF}$ is set to 0.9. In particular, Figure 5(a) shows the active power provided by the V2G station, which depends on its rated power, i.e., 0.27 MW, plus a 1.1 overload factor allowance. Besides, Figure 5(b) shows the *SoC* reduction at EV-level in case 6, 12 or 50 EVs are connected to the station (assuming all EVs have the same battery parametrized later in section IV). As expected, the *SoCs* drop with a linear trend. Moreover, a point worth noting is that even with a small number of connected EVs, an acceptable *SoC* is preserved after 300 s. Therefore, the example shows that it would be beneficial for EVs to participate in frequency regulation, as acceptable final *SOC* levels are maintained.

In addition, Figure 5(a) provides a visual explanation of how the frequency control works. Initially, the injected power remains at zero as the frequency deviation lies within the dead-band limits (see Figure 4). The frequency event occurs at t = 5 s, and the dead-band limit is reached almost immediately. As the initial *SoC* is higher than 0.9, the lower loop of Figure 4 indicated with $-\Delta f$ is followed, and the primary control intervenes. However, a limited amount of power is injected in accordance with the statism level required by the Spanish TSO [34]. After 15 s, the secondary control is activated, and the full available power is injected.

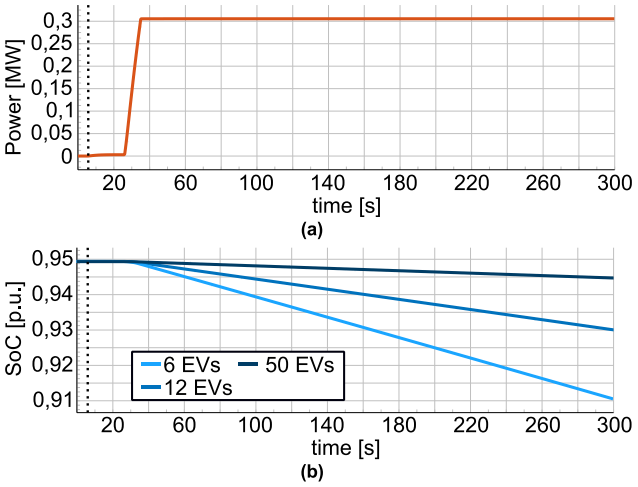

FIGURE 5. Power vs. time and SOC vs. time curves of one 0.4 kV V2G stations in an underfrequency event.

IV. KEY PERFORMANCE INDICATORS

Key Performance Indicators (KPIs) are quantifiable measures used to evaluate the success of a system in meeting its objectives. This work proposes a set of KPIs to evaluate and compare the frequency response in the different V2G installed capacities and aggregation scenarios at HV, MV and LV levels. The following KPIs are evaluated based on the recommendations and guidelines provided in [31] and [37]:

1. Number of V2G (*No V2G*): number of Vehicle-to-Grid chargers actively participating in the frequency event.
2. Steady-state secondary frequency (f_{fin}): final steady-state frequency reached after the secondary control engagement.
3. Frequency nadir (f_{nadir}): minimum value of frequency reached during the transient period, under the effect of the primary control.
4. Frequency correction (Δf): difference between the frequency deviation with and without secondary control. Mathematically, frequency correction is expressed by the following equation:

$$\Delta f = \left|(f_n + f_{deviation}) - f_{fin}\right| \tag{1}$$

where f_n is the system rated frequency, $f_{deviation}$ is the frequency deviation due to frequency event (indicated later in TABLE 3), and f_{fin} is the steady-state secondary frequency.

5. Steady-state power (P_{V2G}): steady-state power provided by all V2G chargers.
6. $\Delta f / P_{V2G}$: ratio between the frequency correction and the active power provided by the V2Gs. Mathematically, $\Delta f / P_{V2G}$ ratio follows the equation:

$$\Delta f / P_{V2G} = \frac{\Delta f \cdot 100}{P_{V2G}} \tag{2}$$

where Δf is the frequency correction and P_{V2G} is the V2Gs' steady-state power.

7. Losses Variation (ΔP_{loss}): active power loss variation inside the electric system due to the power supplied/absorbed by the V2Gs during the frequency event.
8. RoCoF: Rate of Change of Frequency, which can be expressed mathematically as:

$$RoCoF = \frac{df}{dt} = \frac{f_n P}{2HS_b} \tag{3}$$

where f_n is the system rated frequency, P is the lost load/generation, H is the system inertia, and S_b is the base power of the system.

V. WORKING FRAMEWORK DESCRIPTION

This section describes the aforementioned ''global working framework'' developed to analyze the impact on the grid of V2Gs participation in a frequency event. The process is composed of four main steps:

A. Definition of grid topology and available V2Gs locations at HV, MV and LV.
B. Definition of the V2Gs rated power and energy capacities.
C. Frequency event definition.
D. Definition of the Use Cases, i.e., V2Gs overall installed capacities and aggregation amounts at HV, MV and LV.

A. DEFINITION OF GRID TOPOLOGY AND V2Gs AVAILABLE LOCATIONS

As already indicated, this work has been conducted using the reality-based electric system built for the EU-H2020 project INCIT-EV. The model has been developed in DIgSILENT PowerFactory [38]. The network overview is illustrated in Figure 6. As it is shown, the network is composed of different subgrids in high, medium and low voltage. Their description and the available V2G stations are provided below:

1. *HV, 230 kV Equivalent Transmission System.* This subgrid is defined in [39] and used in the Spanish grid code for power oscillations phenomena. No V2G stations have been considered in this subgrid.
2. *HV, 132 kV IEEE 14-node Grid*. This subgrid is defined in [40]. It connects the *HV, 230 kV Equivalent Transmission System* to three MV and ten LV subgrids. Here, V2G stations are connected at 132 kV and 33 kV.
3. *MV, 66 kV inter-urban grid.* This subgrid represents a real network modelled in the project INCIT-EV; V2G stations are available at 20 kV and 0.4 kV.
4. *MV, 10 kV peri-urban grid.* This subgrid also represents a real network modelled in the project INCIT-EV. Here, V2G stations are connected only at 10 kV.
5. *MV, 4.16 kV IEEE 13-node Grid.* This subgrid is modelled according to [41]. In this case, V2G stations are available only at 4.16 kV.
6. *LV, 0.4 kV IEEE European Low Voltage Test Feeder*. This subgrid is modelled according to [41]. As shown in Figure 6, ten test feeders have been connected and grouped five by five. V2G stations are available only at 0.4 kV.

Locations of all available V2Gs in each subgrid are illustrated in Appendix A, along with the subgrids' topologies. These locations have been selected by a combination of real data, literature review and random selection criteria.

B. DEFINITION OF V2Gs RATED POWER AND ENERGY CAPACITIES

In order to provide a reality-based representation of future scenarios, where both slow and fast V2G stations will be connected to the grid, six types of V2G voltage and power ratings have been considered, as reported in Table 1. Selection of V2Gs' voltage levels and power ratings have been conducted by following the same approach adopted to select the V2G locations (real data, literature review and random selection).

For what is concerned with the EVs battery capacity, to avoid overcomplicating the model without losing generality in the results, it has been decided to consider a mid-size battery pack for all EVs. Data have been adapted from a commercial 60-kWh model and are shown in Table 2 [42].

TABLE 1. V2G types: voltage and power ratings.

Subgrid	Rated AC voltage [kV]	Rated DC Voltage [kV]	Rated Power [kW]
LV	0.4	0.7	6.15 – 242
MV #1, IEEE 13-node	4.16	7	246 – 450
MV #2, Peri-urban	10	17	230 – 444
MV #3, Inter-urban	20	33	260 – 350
MV #4, Inter-urban	33	55	606 – 821
HV #1, IEEE 14-node	132	220	682 – 789

C. FREQUENCY EVENT DEFINITION

A load event is generated on the *HV, 230 kV Equivalent Transmission System* (Figure 7) to produce a frequency change in the complete network. The load event is produced by imposing a 60 MW step change in the HV load marked by the dotted red line. Then, this change causes a frequency deviation in absence of regulation of 0.2585 Hz upwards and 0.2629 Hz downwards, as indicated in Table 3. The difference in frequency between the underfrequency and overfrequency events is due to losses in the power grid.

D. V2Gs INSTALLED CAPACITIES AND PENETRATION SCENARIOS

To complete the description of the ''global working framework'', as the complete grid topology has been defined and V2Gs locations identified, relevant Use Cases (UCs) are now defined. In particular, UCs studied in this work are classified according to the type of frequency deviation:

A. Underfrequency event.
B. Overfrequency event.

Subsequently, in each UC, two installed V2G capacities are studied, which are as follows:

1. 10 MW.
2. 20 MW.

Finally, for each UC and both installed capacities, four different aggregation scenarios are studied. In particular, aggregation scenarios are defined according to the amount of V2G capacity aggregated from the HV, MV and LV subgrids, as summarized in Table 4.

VI. RESULTS AND DISCUSSION

The results have been obtained by simulating in DIgSILENT PowerFactory the network and the scenarios described in section V.

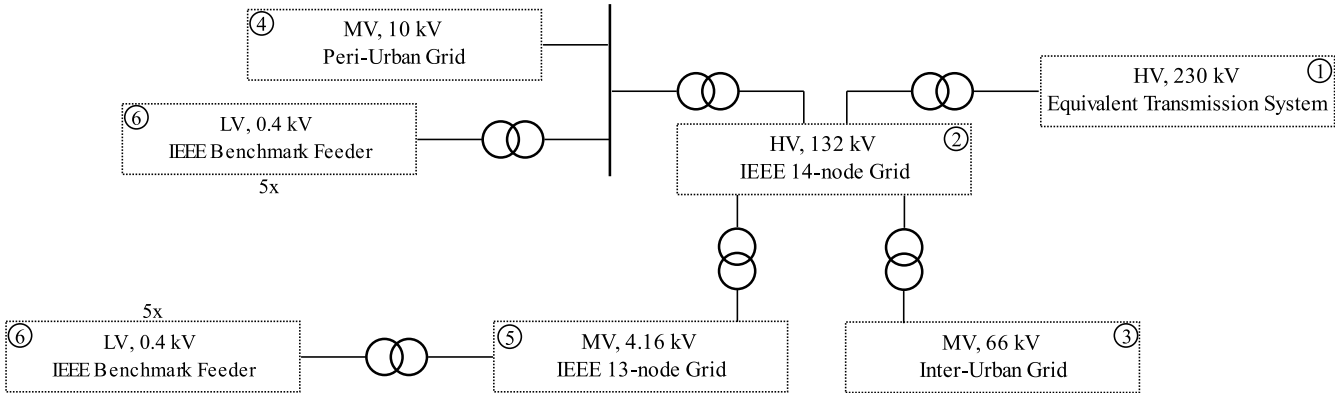

FIGURE 6. Reality-based electric network modelled in the EU-H2020 project INCIT-EV.

TABLE 2. EVs battery pack characteristics.

Quantity	Value
Overall capacity [kWh]	60
Rated pack DC voltage [kV]	0.4
Number of cells in series	96
Number of cells in parallel	3

TABLE 3. Load step generating the frequency event.

HV Load Value [MW]	Load Step [MW]	Frequency Deviation [Hz]
4000	+ 60	- 0.2585
4000	- 60	+ 0.2629

TABLE 4. Scenarios: V2Gs aggregation shares.

Scenario	% HV	% MV	% LV
1	0	40	60
2	0	60	40
3	100	0	0
4	33	33	33

FIGURE 7. *HV, 230 kV equivalent transmission system* and HV load event.

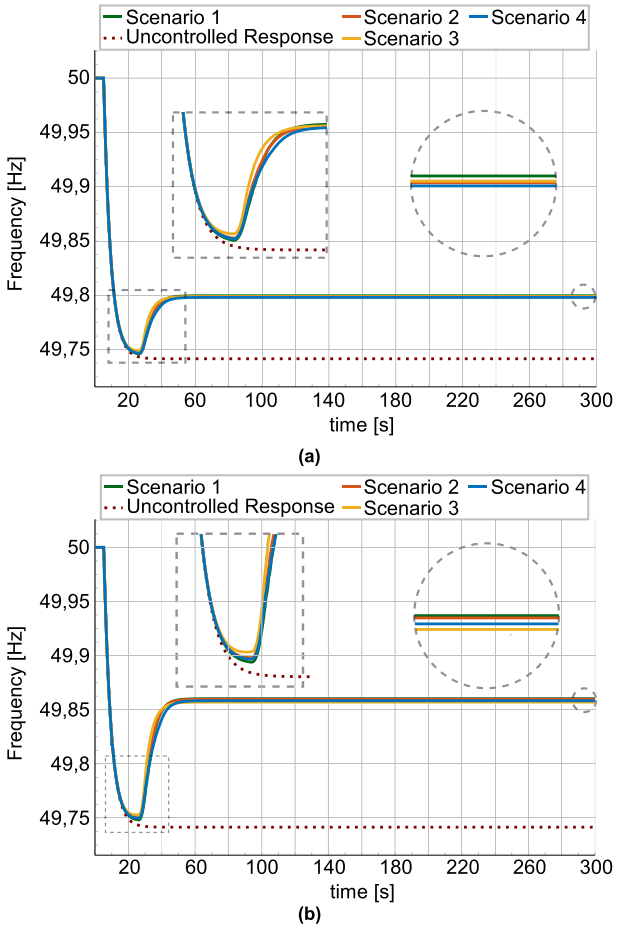

FIGURE 8. Frequency evolution in the underfrequency event with V2G installed capacity of a) 10 MW, b) 20 MW.

A. UC1: UNDERFREQUENCY EVENT RESULTS AND ANALYSIS

Figure 8(a) and (b) compare the four frequencies vs time response curves against the uncontrolled response for both installed capacities. In both figures, frequency nadir regions and the final stabilized frequency are zoomed in.

KPIs are summarized in Table 5 for the 10 MW case and Table 6 for 20 MW.

As can be seen, scenarios 1, 2, and 4 achieve a similar nadir value. However, scenario 3 shows the highest nadir, meaning that the primary control has a more relevant effect when EVs are aggregated only from the HV subgrid, com-

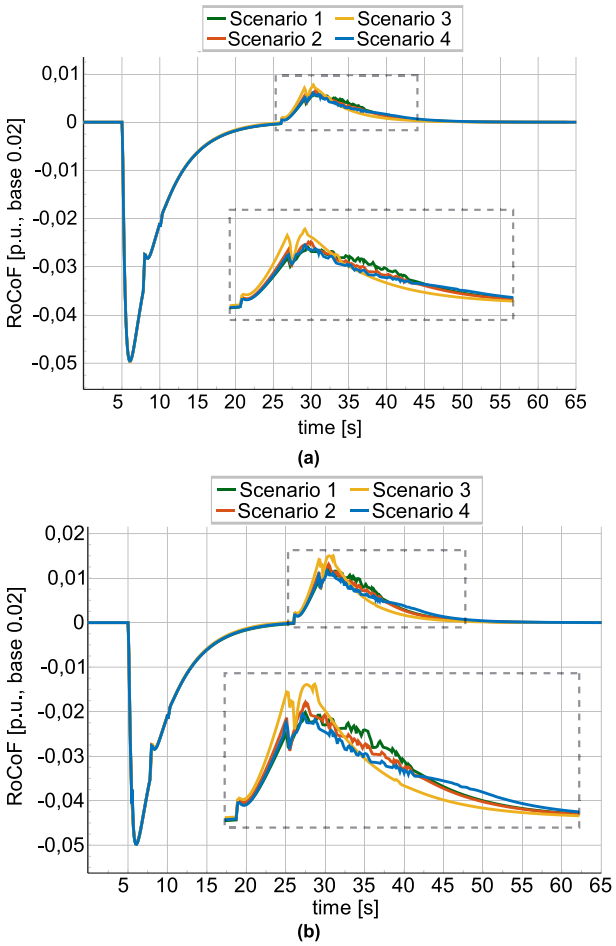

FIGURE 9. RoCoF evolution in the underfrequency event with V2G installed capacity of a) 10 MW, b) 20 MW.

pared to the other cases where LV and MV subgrids are also involved. Regarding the steady-state secondary frequency (f_{fin}), in both V2G installed capacities, scenario 1 (no HV aggregation) obtains the highest frequency increase and, therefore, a higher f_{fin}.

Furthermore, the RoCoF is evaluated graphically in Figure 9 for both installed capacities. In general terms, a relatively reduced effect of the V2Gs over RoCoF and Nadir is observed, due to the very low contribution provided by the primary controller in accordance with [34]. Regarding voltage level distributions, scenarios 1, 2, and 4 show similar behavior, as they reach approximately the same minimum value and stabilize simultaneously. Conversely, scenario 3 provides controversial results, as it reaches the highest RoCoF, although frequency stabilizes earlier. This observation yields further critical insight. The difference in RoCoF between the scenarios at hand shows that the amount of V2Gs aggregated at HV, MV, and LV levels has a noticeable effect on the virtual or synthetic inertia provided by the EV fleet. This aspect will be investigated further in future works.

Another point to highlight concerns the 6th KPI $\Delta f/P_{V2G}$, which expresses the effectiveness of each kW

TABLE 5. KPIs summary for 10 MW V2G installed capacity, underfrequency.

	Scenario 1	Scenario 2	Scenario 3	Scenario 4
No. V2G	56	51	10	44
f_{fin} [Hz]	49.7996	49.7987	49.7988	49.7981
Nadir [Hz]	49.746	49.747	49.749	49.747
Δf [Hz]	0.0581	0.0572	0.0573	0.0566
P_{V2G} [MW]	10.81	10.71	10.57	10.65
$\Delta f/P_{V2G}$ [Hz*100/MW]	0.538	0.534	0.542	0.532
ΔP_{loss} [MW]	0.13	0.18	-0.01	0.20

TABLE 6. KPIs summary for 20 MW V2G installed capacity, underfrequency.

	Scenario 1	Scenario 2	Scenario 3	Scenario 4
No. V2G	100	93	10	74
f_{fin} [Hz]	49.8602	49.8596	49.8570	49.8583
Nadir [Hz]	49.748	49.750	49.753	49.750
Δf[Hz]	0.1187	0.1181	0.1155	0.1168
P_{V2G} [MW]	21.83	21.78	21.27	21.69
$\Delta f/P_{V2G}$ [Hz*100/MW]	0.544	0.542	0.543	0.538
ΔP_{loss} [MW]	0.56	0.59	0.45	0.73

generated/absorbed by the EV fleet in correcting the frequency deviation. Here, the first observation stems from the scale factor. In scenarios 1, 2 and 4, $\Delta f/P_{V2G}$ increases when higher power is aggregated, i.e., from 10 MW to 20 MW. In contrast, $\Delta f/P_{V2G}$ remains almost equal in scenario 3, regardless of the aggregated power variation. This trend may be explained by observing that in scenarios 1, 2 and 4 most EV stations are located in the LV and MV subgrids. Therefore, if capacity is increased along with the number of EV stations, local generation/consumption is also enhanced because charging stations are closer to the consumers and can feed them directly. Consequently, as local generation / utilization of electric power increases, transportation for long distances through the electric system is no longer necessary, avoiding the corresponding losses and thus improving the frequency correction effectiveness.

Regarding the losses variation ΔP_{loss}, similar considerations can be made. Firstly, it can be noted that loss variation increases by approximately a factor of 4 when the EVs aggregation capacity doubles, suggesting a quadratic trend. Here, scenario 3 features the lowest losses, as all the EV penetration and, therefore, all the additional power supplied into the electric system is at the HV level. Indeed, the loss variation is even negative in scenario 3 with a 10 MW V2G installed capacity. The negative value indicates that with the V2Gs power supply, load flow restructures so that the losses in the grid are lower than without them.

A final point worth noting is that the overall perceived worst case is scenario 4, which features the lowest $\Delta f/PV2G$ ratio and the highest losses. This is due to the fact that EV

penetration is highly distributed within the electric system, and MV penetration predominates. This, in turn, leads to higher electric power transportation through the electric grid, which minimizes the frequency correction effectiveness.

As an example of the way load flow restructures in the network, the case of 10 MW V2G installed capacity and underfrequency event is now analyzed in more detail. Table 7 and Table 8 summarize, respectively, the active power flow and losses restructuration in the interconnection lines of each subgrid (see Figure 6), for each scenario, after 300s of simulation and with the secondary control contribution. The pre-fault conditions, i.e., before the V2Gs power contribution, are also included. As can be seen in Table 7, the power flow restructuring depends on the location of the V2Gs. For example, scenario 3 significantly impacts on the power flow restructuring in the HV network, being negligible in the other ones. It should also be noted that the power flow restructuring causes a change of sign in scenarios 1, 2, and 4 in all subgrids, excluding the MV 10 kV one. This means the overall subgrids' behavior switches from absorbing to generating power. In particular, apart from the change in sign, in the MV 4.16 kV subgrid a considerable increase in power flow is observed, as it is now transporting the power contributions of five LV subgrids.

TABLE 7. Subgrids interconnection lines, active power flow in underfrequency event [MW].

	Pre-Fault	Scenario 1	Scenario 2	Scenario 3	Scenario 4
HV 132 kV	47	36.33	36.47	37.52	36.56
MV 66 kV	1.4	-3.2	-1.85	1.32	-0.52
MV 10 kV	14.24	12.15	11.53	14.34	11.91
MV 4.16 kV	0.71	-2.54	-3.05	0.71	-3.2
LV 0.4 kV	0.002	-0.038	-0.038	0.002	-0.038

TABLE 8. Subgrids interconnection lines, losses in underfrequency event [kW].

	Pre-Fault	Scenario 1	Scenario 2	Scenario 3	Scenario 4
HV 132 kV	344.04	216.52	216.47	224.21	215.85
MV 66 kV	389.76	312.85	317.37	322.98	313.97
MV 10 kV	119.41	85.40	77.28	120.26	80.58
MV 4.16 kV	11.62	36.35	47.83	11.65	51.87
LV 0.4 kV	0.001	0.004	0.004	0.001	0.004

Besides, Table 8 summarizes the losses in each subgrid interconnection line. According to what was observed above, power losses increase in the MV 4.16 kV subgrid as a consequence of the increase in power flow, whereas losses decrease in almost all subgrids in all scenarios. In scenario 3, a significant decrease in losses is obtained only in the HV subgrid. This is because the V2Gs are connected near the fault location and hence feed it directly. Overall, losses in scenario 2 are slightly higher than in scenario 1, with scenario 4 as the worst-case.

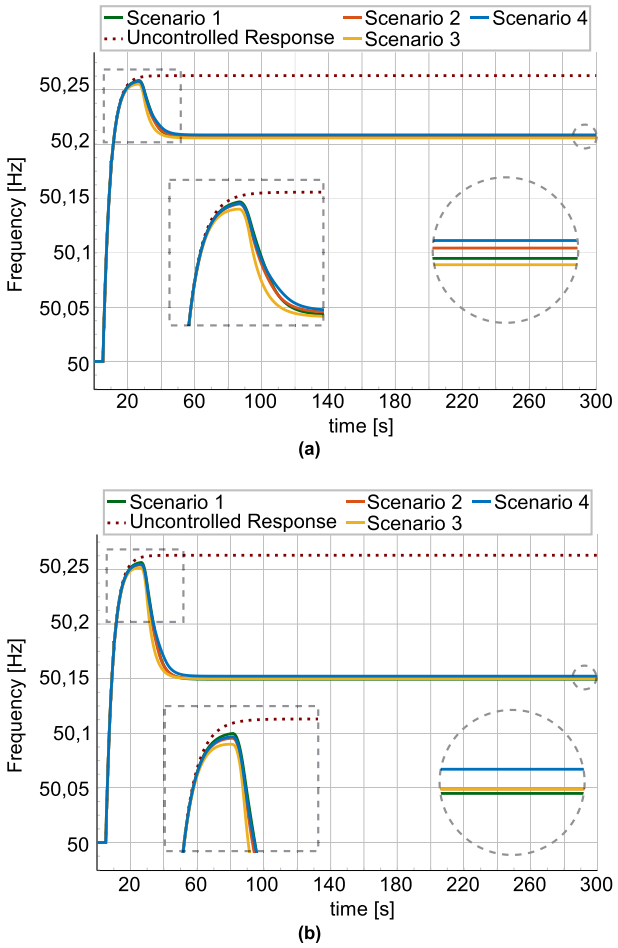

FIGURE 10. Frequency evolution in the overfrequency event with V2G installed capacity of a) 10 MW, b) 20 MW.

All the above concludes that local generation / consumption of electric power is a highly effective way of correcting frequency deviations through fleets of plugged-in EVs. Therefore, it would be essential to consider it during the aggregation process. It is worth noting that this conclusion could not be easily demonstrated without modelling the entire electric system, as has been proposed in this work.

B. UC2: OVERFREQUENCY EVENT RESULTS AND ANALYSIS

As per the underfrequency UC, two V2G installed capacities and four voltage-dependent aggregation scenarios have been simulated in DIgSILENT PowerFactory.

Figure 10 compares the four frequencies vs time response curves against the uncontrolled response for both installed capacities. Frequency nadir regions and the final stabilized frequency are zoomed in.

The nadir region shows similar results as those obtained in the underfrequency UC, reaching the lowest value in scenario 3. As per the stabilized frequency, the worst value is reached in scenario 4, while scenarios 1, 2 and 3 give similar results and achieve a similar frequency reduction. As for the RoCoF, results are similar to those of underfrequency, as it

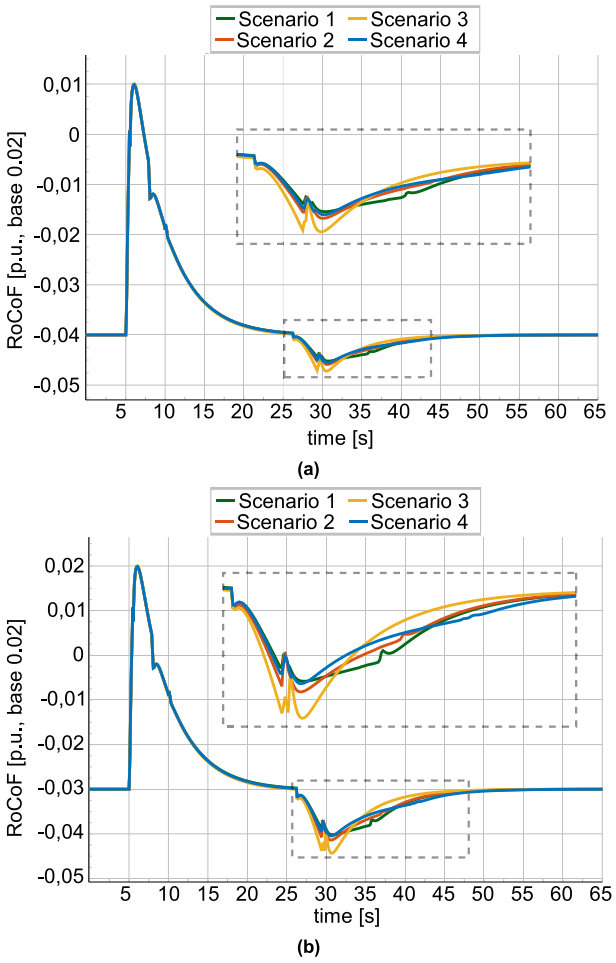

FIGURE 11. RoCoF evolution in the overfrequency event with V2G installed capacity of a) 10 MW, b) 20 MW.

is shown in Figure 11. KPIs are summarized in Table 9 for the 10 MW case and Table 10 for 20 MW.

TABLE 9. KPIS summary for 10 MW V2G installed capacity, overfrequency.

	Scenario 1	Scenario 2	Scenario 3	Scenario 4
No. V2G	56	51	10	44
f_{fin} [Hz]	50.2064	50.2076	50.2057	50.2084
Nadir [Hz]	50.259	50.528	50.255	50.258
Δf [Hz]	0.0565	0.0553	0.0573	0.0545
P_{V2G} [MW]	10.40	10.27	10.53	10.17
$\Delta f/P_{V2G}$ [Hz*100/MW]	0.543	0.539	0.544	0.536
ΔP_{loss} [MW]	-0.03	0.02	0.015	0.05

As for the underfrequency UC, 10 MW and 20 MW installed capacities give relatively similar results. However, a few key insights are provided in the following.

In this UC, EV chargers do not turn from loads to generators but increase the overall load level. Consequently, the local power generation/consumption principle discussed for the underfrequency case is no longer so straightforward.

TABLE 10. KPIS summary for 20 MW V2G installed capacity, overfrequency.

	Scenario 1	Scenario 2	Scenario 3	Scenario 4
No. V2G	100	93	10	74
f_{fin} [Hz]	50.1495	50.1500	50.1500	50.1523
Nadir [Hz]	50.256	50.254	50.251	50.255
Δf [Hz]	0.1134	0.1129	0.1129	0.1106
P_{V2G} [MW]	20.86	20.79	20.87	20.46
$\Delta f_{fin}/P_{V2G}$ [Hz*100/MW]	0.544	0.543	0.541	0.540
ΔP_{loss} [MW]	0.40	0.42	0.55	0.43

In fact, by observing the $\Delta f/P_{V2G}$ values at 10 MW and 20 MW, different trends may be detected, as the KPI reduces for scenario 3, remains equal in scenario 1 and increases in scenarios 2 and 4.

Regarding the losses variation ΔP_{loss}, in this case, the key point to observe is that very low values are obtained with a 10 MW, whereas similar values to the underfrequency case are found for 20 MW capacity. Further effort is therefore needed to gain a deeper insight and thus predict the losses behavior in overfrequency events. Finally, as in the underfrequency UC, the perceived worst case remains scenario 4, confirming the poor effectiveness of a scattered aggregation of EVs at all voltage levels.

C. RESULTS DISCUSSION, RECOMMENDATIONS AND NEXT STEPS

After analyzing the results obtained for underfrequency and overfrequency use cases, the key findings can be summarized as follows.

Firstly, a relatively low number of EVs can provide a non-negligible frequency correction with an acceptable variation of the SoC.

Secondly, a change in the number of V2Gs aggregated at HV, MV, and LV levels has a substantial impact on the way the frequency event is tackled in terms of effectiveness ($\Delta f/P_{V2G}$), efficiency (P_{loss}) and inertia (RoCoF).

In particular, in the case of underfrequency events, the most effective ways are either the aggregation at LV level, as it maximizes local electricity generation/consumption and hence minimizes the need to transport electricity for long distances and/or the aggregation at HV level. Finally, it has been found that scenario 4, i.e., 33% of EVs aggregated at HV, MV and LV levels, is the worst option possible. This suggests that aggregating EVs at the MV level is less effective for tackling a frequency deviation. Based on the above, the following recommendations can be given regarding the aggregation strategy:

- It is essential to simulate all voltage levels of the electric system to select the optimum number of EVs for each of them. In other words, aggregated or "local" models pose the risk of losing critical information.
- Aggregation at the MV level should be avoided as much as possible. This recommendation could be translated

into economic actions, such as lower compensation tariffs or penalizations for EVs aggregated at MV.
- In case an optimization algorithm is being developed, the analysis conducted in this work may provide valuable guidelines. For example, if the objective function is loss minimization, aggregation at HV should be prioritized. Conversely, if the objective function is the maximization of $\Delta f/P_{V2G}$, which would minimize both the SoC variation and the economic compensation to the EV owners, the optimal share between HV and LV need to be determined.

Based on the outcome of the analysis discussed above, future work will focus on developing new aggregation algorithms that take into account all system voltage levels and investigate voltage-level-based remuneration schemes for EV owners. Furthermore, new studies will be conducted with different penetration scenarios considering only HV and LV levels, extending the focus to very low-inertia systems and/or isolated grid-connected V2Gs.

VII. CONCLUSION

This work analyses the grid impact of V2G participation in a frequency event using a ''global working framework'', where two HV transmission, three MV subtransmission and ten LV distribution subgrids are interconnected. Then, the amount of V2Gs aggregated at HV, MV and LV levels has been changed, along with the power and energy capacities. Finally, several Key Performance Indicators (KPIs) have been set to analyze and compare the results. The main conclusions of this work have been reported and discussed in section VI-C and can be summarized as follows.

Firstly, a relatively low number of V2Gs is sufficient to contribute to a frequency event. Secondly, simulating all voltage levels of the electric system is critical for achieving an optimized aggregation process. Thirdly, this work demonstrated that local generation / consumption and hence the minimization of electricity transportation for long distances provides a highly effective solution for frequency deviation correction. On the other hand, this work has also shown that the worst perceived solution is to aggregate V2Gs in a distributed way, i.e., similar amounts of power from HV, MV and LV levels. Based on the three points above, a set of recommendations and guidelines has been provided in section VI-C.

APPENDIX

This Appendix provides a visual overview of all subgrids composing the electric network modelled in the EU-H2020 project INCIT-EV used in this work. All subgrids are illustrated in Figure 12 to Figure 16. Locations of all available V2G stations are also represented as colored rectangles.

A. HV, 230 kV EQUIVALENT TRANSMISSION SYSTEM

The topology of the equivalent 230-kV transmission system used in the Spanish grid code for studying power oscillations

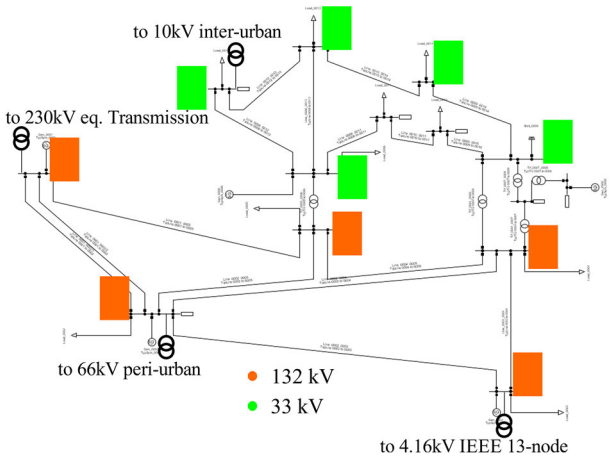

FIGURE 12. 230 kV HV, 132 kV IEEE 14-node grid modelled in DIgSILENT PowerFactory with V2G locations.

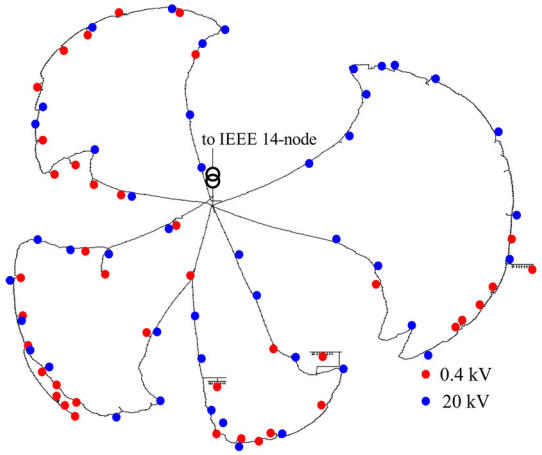

FIGURE 13. Real 10 kV, MV peri-urban grid modelled in DIgSILENT PowerFactory with V2G locations.

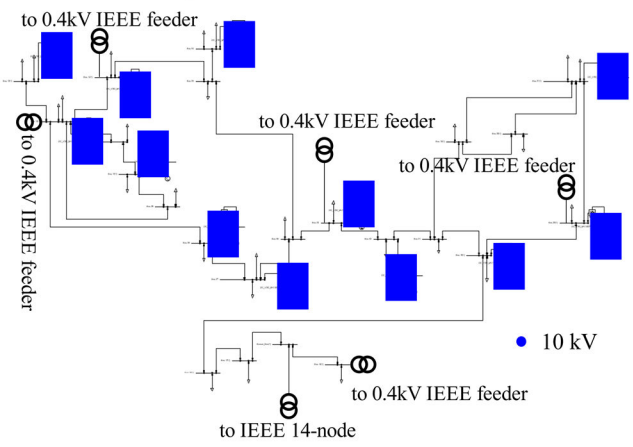

FIGURE 14. Real 66 kV, MV inter-urban grid modelled in DIgSILENT PowerFactory with V2G locations.

phenomena has already been shown in Figure 7. Its main data are reported in Table 11.

It is essential to observe that an external grid has been used instead of a slack synchronous generator. This choice has

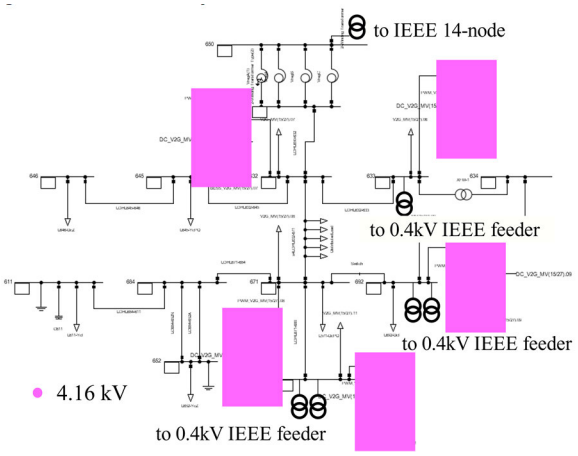

FIGURE 15. MV, 4.16 kV IEEE 13-node grid modelled in DIgSILENT PowerFactory with V2G locations.

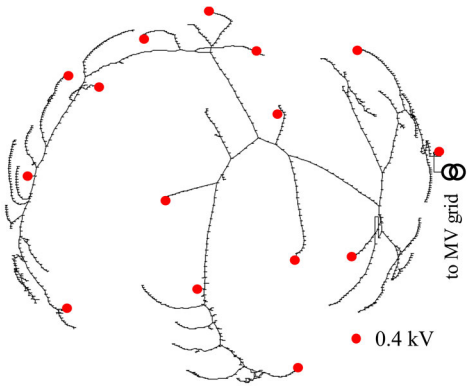

FIGURE 16. LV, 0.4 kV IEEE european low voltage test feeder modelled in DIgSILENT PowerFactory with V2G locations.

TABLE 11. 230-KV system main data.

Quantity	Value
Line impedance [Ω]	176.3
External grid frequency bias [MW/Hz]	50
External grid acceleration time constant [s]	0.5

been made since the external grid allows one to set the acceleration time constant, which refers to the mechanical starting time and is equal to twice the inertia time constant. Moreover, the external grid permits defining the secondary frequency bias (MW/Hz). This parameter is used to calculate the droop characteristics (output of the internal speed controller) used for the simulations.

REFERENCES

[1] S. P. Surve, R. Rocca, E. J. Engeveld, D. Martínez, M. P. Comech, and D. M. Rivas, "Impact assessment of different battery energy storage technologies in distribution grids with high penetration of renewable energies," *Renew. Energy Power Qual. J.*, vol. 20, pp. 650–655, Sep. 2022, doi: 10.24084/repqj20.391.

[2] R. Rocca, S. Papadopoulos, M. Rashed, G. Prassinos, F. G. Capponi, and M. Galea, "Design trade-offs and feasibility assessment of a novel one-body, laminated-rotor flywheel switched reluctance machine," *Energies*, vol. 13, no. 22, p. 5857, Nov. 2020, doi: 10.3390/en13225857.

[3] B. Bibak and H. Tekiner-Mogulkoç, "A comprehensive analysis of vehicle to grid (V2G) systems and scholarly literature on the application of such systems," *Renew. Energy Focus*, vol. 36, pp. 1–20, Mar. 2021, doi: 10.1016/j.ref.2020.10.001.

[4] M. Marinelli, L. Calearo, S. Ried, X. Pfab, J. C. Diaz Cabrera, C. Spalthoff, M. Braun, H. Sæle, B. N. Torsæter, P. H. Divshali, S. Hänninen, M. Ceraolo, S. Barsali, M. Larsson, A. Magdowski, L. Gimenez, and G. Fernández, "Electric vehicles demonstration projects—An overview across Europe," in *Proc. 55th Int. Universities Power Eng. Conf. (UPEC)*, Sep. 2020, pp. 1–6, doi: 10.1109/UPEC49904.2020.9209862.

[5] M. Tamba, J. Krause, M. Weitzel, R. Ioan, L. Duboz, M. Grosso, and T. Vandyck, "Economy-wide impacts of road transport electrification in the EU," *Technological Forecasting Social Change*, vol. 182, Sep. 2022, Art. no. 121803, doi: 10.1016/j.techfore.2022.121803.

[6] J. Engelhardt, J. M. Zepter, T. Gabderakhmanova, and M. Marinelli, "Energy management of a multi-battery system for renewable-based high power EV charging," *eTransportation*, vol. 14, Nov. 2022, Art. no. 100198, doi: 10.1016/j.etran.2022.100198.

[7] M. Ledro, L. Calearo, J. M. Zepter, T. Gabderakhmanova, and M. Marinelli, "Influence of realistic EV fleet response with power and energy controllers in an EV-wind virtual power plant," *Sustain. Energy, Grids Netw.*, vol. 31, Sep. 2022, Art. no. 100704, doi: 10.1016/j.segan.2022.100704.

[8] S. Leonori, G. Rizzoni, F. M. Frattale Mascioli, and A. Rizzi, "Intelligent energy flow management of a nanogrid fast charging station equipped with second life batteries," *Int. J. Electr. Power Energy Syst.*, vol. 127, May 2021, Art. no. 106602, doi: 10.1016/j.ijepes.2020.106602.

[9] B. K. Sovacool and R. F. Hirsh, "Beyond batteries: An examination of the benefits and barriers to plug-in hybrid electric vehicles (PHEVs) and a vehicle-to-grid (V2G) transition," *Energy Policy*, vol. 37, no. 3, pp. 1095–1103, Mar. 2009, doi: 10.1016/j.enpol.2008.10.005.

[10] B. Tarroja, L. Zhang, V. Wifvat, B. Shaffer, and S. Samuelsen, "Assessing the stationary energy storage equivalency of vehicle-to-grid charging battery electric vehicles," *Energy*, vol. 106, pp. 673–690, Jul. 2016, doi: 10.1016/j.energy.2016.03.094.

[11] M. H. Khooban, "An optimal non-integer model predictive virtual inertia control in inverter-based modern AC power grids-based V2G technology," *IEEE Trans. Energy Convers.*, vol. 36, no. 2, pp. 1336–1346, Jun. 2021, doi: 10.1109/TEC.2020.3030655.

[12] C. O'Malley, L. Badesa, F. Teng, and G. Strbac, "Frequency response from aggregated V2G chargers with uncertain EV connections," *IEEE Trans. Power Syst.*, vol. 38, no. 4, pp. 3543–3556, Jul. 2023, doi: 10.1109/TPWRS.2022.3202607.

[13] A. Naveed, S. Sönmez, and S. Ayasun, "Impact of electric vehicle aggregator with communication time delay on stability regions and stability delay margins in load frequency control system," *J. Modern Power Syst. Clean Energy*, vol. 9, no. 3, pp. 595–601, May 2021, doi: 10.35833/MPCE.2019.000244.

[14] C. Dong, J. Sun, F. Wu, and H. Jia, "Probability-based energy reinforced management of electric vehicle aggregation in the electrical grid frequency regulation," *IEEE Access*, vol. 8, pp. 110598–110610, 2020, doi: 10.1109/ACCESS.2020.3002693.

[15] H. Liu, Z. Hu, Y. Song, and J. Lin, "Decentralized vehicle-to-grid control for primary frequency regulation considering charging demands," *IEEE Trans. Power Syst.*, vol. 28, no. 3, pp. 3480–3489, Aug. 2013, doi: 10.1109/TPWRS.2013.2252029.

[16] O. Kolawole and I. Al-Anbagi, "Electric vehicles battery wear cost optimization for frequency regulation support," *IEEE Access*, vol. 7, pp. 130388–130398, 2019, doi: 10.1109/ACCESS.2019.2930233.

[17] K. Kaur, N. Kumar, and M. Singh, "Coordinated power control of electric vehicles for grid frequency support: MILP-based hierarchical control design," *IEEE Trans. Smart Grid*, vol. 10, no. 3, pp. 3364–3373, May 2019, doi: 10.1109/TSG.2018.2825322.

[18] J. Donadee and M. D. Ilic, "Stochastic optimization of grid to vehicle frequency regulation capacity bids," *IEEE Trans. Smart Grid*, vol. 5, no. 2, pp. 1061–1069, Mar. 2014, doi: 10.1109/TSG.2013.2290971.

[19] K. S. Ko, S. Han, and D. K. Sung, "A new mileage payment for EV aggregators with varying delays in frequency regulation service," *IEEE Trans. Smart Grid*, vol. 9, no. 4, pp. 2616–2624, Jul. 2018, doi: 10.1109/TSG.2016.2614815.

[20] E. Yao, V. W. S. Wong, and R. Schober, "Robust frequency regulation capacity scheduling algorithm for electric vehicles," *IEEE Trans. Smart Grid*, vol. 8, no. 2, pp. 984–997, Mar. 2017, doi: 10.1109/TSG.2016.2530660.

[21] A. Thingvad, L. Calearo, P. B. Andersen, M. Marinelli, M. Neaimeh, K. Suzuki, and K. Murai, "Value of V2G frequency regulation in great Britain considering real driving data," in *Proc. IEEE PES Innov. Smart Grid Technol. Eur. (ISGT-Europe)*, Sep. 2019, pp. 1–5, doi: 10.1109/ISGTEurope.2019.8905679.

[22] S. Gao, H. Li, J. Jurasz, and R. Dai, "Optimal charging of electric vehicle aggregations participating in energy and ancillary service markets," *IEEE J. Emerg. Sel. Topics Ind. Electron.*, vol. 3, no. 2, pp. 270–278, Apr. 2022, doi: 10.1109/jestie.2021.3102417.

[23] J. D. Fitzsimmons, S. J. Kritzer, V. A. Muthiah, J. J. Parmer, T. J. Rykal, M. T. Stone, M. C. Brannon, J. P. Wheeler, D. L. Slutzky, and J. H. Lambert, "Simulation of an electric vehicle fleet to forecast availability of grid balancing resources," in *Proc. IEEE Syst. Inf. Eng. Design Symp. (SIEDS)*, Apr. 2016, pp. 205–210, doi: 10.1109/SIEDS.2016.7489300.

[24] C. H. Merrill, V. H. Lam, M. J. Van Vleet, M. S. Chatti, M. C. Brannon, E. B. Connelly, J. H. Lambert, D. L. Slutzky, and J. P. Wheeler, "Modeling and simulation of fleet vehicle batteries for integrated logistics and grid services," in *Proc. Syst. Inf. Eng. Design Symp.*, Apr. 2015, pp. 255–260, doi: 10.1109/SIEDS.2015.7116985.

[25] P. Jampeethong and S. Khomfoi, "Coordinated control of electric vehicles and renewable energy sources for frequency regulation in microgrids," *IEEE Access*, vol. 8, pp. 141967–141976, 2020, doi: 10.1109/ACCESS.2020.3010276.

[26] S. Iqbal, A. Xin, M. U. Jan, M. A. Abdelbaky, H. U. Rehman, S. Salman, S. A. A. Rizvi, and M. Aurangzeb, "Aggregation of EVs for primary frequency control of an industrial microgrid by implementing grid regulation & charger controller," *IEEE Access*, vol. 8, pp. 141977–141989, 2020, doi: 10.1109/ACCESS.2020.3013762.

[27] I. A. Walton, K. W. Diduch, A. H. Kim, S. B. Lockett, J. M. O'Rourke, T. Sinha, A. B. Korbatov, C. J. Steers, J. P. Wheeler, D. L. Slutzky, and J. H. Lambert, "Statistical analysis of building energy load profiles to assess site-specific feasibility of demand charge management," in *Proc. Syst. Inf. Eng. Design Symp. (SIEDS)*, Apr. 2018, pp. 231–236, doi: 10.1109/SIEDS.2018.8374742.

[28] J. R. Pillai and B. Bak-Jensen, "Integration of vehicle-to-grid in the western Danish power system," *IEEE Trans. Sustain. Energy*, vol. 2, no. 1, pp. 12–19, Jan. 2011, doi: 10.1109/TSTE.2010.2072938.

[29] B. Alharbi and D. Jayaweera, "Impact assessment of plug-in electric vehicle charging locations on power systems with integrated wind farms incorporating dynamic thermal limits," *J. Modern Power Syst. Clean Energy*, vol. 10, no. 3, pp. 710–718, May 2022, doi: 10.35833/MPCE.2020.000445.

[30] *Incit-EV*. Accessed: Jul. 1, 2023. [Online]. Available: https://www.incit-ev.eu/deliverables-2

[31] R. Rajan, F. M. Fernandez, and Y. Yang, "Primary frequency control techniques for large-scale PV-integrated power systems: A review," *Renew. Sustain. Energy Rev.*, vol. 144, Jul. 2021, Art. no. 110998, doi: 10.1016/j.rser.2021.110998.

[32] Z. A. Obaid, L. M. Cipcigan, L. Abrahim, and M. T. Muhssin, "Frequency control of future power systems: Reviewing and evaluating challenges and new control methods," *J. Modern Power Syst. Clean Energy*, vol. 7, no. 1, pp. 9–25, Jan. 2019, doi: 10.1007/s40565-018-0441-1.

[33] J. Zhang, J. Liang, H. Chen, S. Zhai, D. He, and J. Xu, "Secondary frequency modulation control strategy of power system using energy storage battery," in *Proc. 7th Int. Conf. Power Renew. Energy (ICPRE)*, Sep. 2022, pp. 396–401, doi: 10.1109/ICPRE55555.2022.9960482.

[34] *BOE Num. 197, P.O. 7.1 Servicio Complementario De Regulación Primaria*, Spanish Ministry Ind. Energy, Madrid, Spain, Aug. 1998.

[35] *BOE Num. 75, P.O. 7.2 Servicio Complementario De Regulación Secundaria*, Spanish Ministry Ind. Energy, Madrid, Spain, Mar. 2022.

[36] *Application Example Battery Energy Storing Systems*, DIgSILENT GmbH, Gomaringen, Germany.

[37] *UCTE Operation Handbook—Appendix 1: Load-Frequency Control and Performance Organisation*, ENTSO-e, Brussels, Belgium, 2004.

[38] DIgSILENT GmbH. Accessed: Jul. 1, 2023. [Online]. Available: https://www.digsilent.de/en/powerfactory.html

[39] *Norma técnica de Supervisión de la Conformidad de Los módulos de Generación de Electricidad Según el Reglamento UE 2016/631, Revisión 2.1*, Red Eléctrica de España (REE), Madrid, Spain, 2021.

[40] S. Monemi, T. Dent, and A. Nunez, "A model of system protection in IEEE 14-bus power grid," in *Proc. IEEE Int. Conf. Power Eng. Appl. (ICPEA)*, Mar. 2022, pp. 1–5, doi: 10.1109/ICPEA53519.2022.9744697.

[41] W. H. Kersting, "Radial distribution test feeders," *IEEE Trans. Power Syst.*, vol. 6, no. 3, pp. 975–985, Aug. 1991, doi: 10.1109/59.119237.

[42] C. Iclodean, B. Varga, N. Burnete, D. Cimerdean, and B. Jurchis, "Comparison of different battery types for electric vehicles," *IOP Conf. Ser., Mater. Sci. Eng.*, vol. 252, Oct. 2017, Art. no. 012058, doi: 10.1088/1757-899X/252/1/012058.

MARTA BERNAL-SANCHO received the B.S. and M.S. degrees in industrial engineering from the University of Zaragoza, Zaragoza, Spain, in 2017 and 2019, respectively, where she is currently pursuing the Ph.D. degree in power control and frequency oscillation control and damping with the CIRCE Research Centre, CIRCE Mixed Research Institute.

Since 2020, she has been a Research Fellow with the Research Centre for Energy Resources and Consumption (CIRCE), Zaragoza, in both EU-funded and national-funded projects in the fields of renewable energies integration and smart grid, such as FARCROSS, eFORT, or private-funded technology transfer projects, such as inter-area oscillation dumping. She is currently a Project Manager of the Electric Networks Operation and Planning Team, CIRCE. Her research interests include power oscillation damping controllers, dynamic modeling and controller's development, renewable energy, FACTS control development, and hardware in the loop (HIL) simulations.

ROBERTO ROCCA (Member, IEEE) was born in Rome, Italy, in 1989. He received the B.S. degree in energy engineering and the M.S. degree in electrical engineering from the Sapienza University of Rome, Rome, Italy, in 2013 and 2015, respectively, and the Ph.D. degree in electrical and electronics engineering from the Power Electronics, Machines and Control Group (PEMC), University of Nottingham, Nottingham, U.K., in 2020.

From 2019 to 2020, he was a Postdoctoral Researcher with the Sapienza Electrical Machines and Power Electronics Research Group (SEMPER), Sapienza University of Rome. He is currently a Research Fellow with the Research Centre for Energy Resources and Consumption (CIRCE), Zaragoza, Spain, and an Adjunct Research Fellow with the CIRCE Research Centre, CIRCE Mixed Research Institute, University of Zaragoza, Zaragoza. His research interests include the modeling and design of electrical machines and drives, novel energy storage systems, the management and optimization of multi-energy districts, local energy communities, and low-inertia transmission networks.

Dr. Rocca was a recipient of the Excellent Paper Award in the ICEMS 2020 Congress and the 2022 IEEE PES Spanish Chapter Outstanding Volunteer Award. He is also a member of the IEEE Power and Energy Society, where he is also the Secretary of the Spanish Chapter.

GREGORIO FERNÁNDEZ-AZNAR received the B.S. degree in industrial engineering with specialization in electrical systems from the University of Zaragoza, Zaragoza, Spain, in 2010, and the M.S. degree in renewable energies from the CIRCE Research Centre, CIRCE Mixed Research Institute, University of Zaragoza, in 2011. He is currently pursuing the Ph.D. degree in the grid integration of electric vehicles charging points.

He is currently a Research Fellow and a Research and Development Project Manager with the Research Centre for Energy Resources and Consumption (CIRCE), Zaragoza, where he is responsible for the execution and management of several projects in the fields of energy storage integration and renewable energies, smart grid projects, such as PARITY, SYNERGY, EV_OPTIMANAGER, FLEXICIENCY, WAVE, FLEXCOOP, MIRED-CON, and electric-vehicle projects, such as INCIT-EV, SIRVE o CRAVE. Since 2012, he has been an Adjunct Lecturer in integration of renewable energies and electric mobility in several M.S. courses provided by CIRCE, EUREC, and the University of Zaragoza. His research interests include integration, optimization and forecasting algorithms in the smart-grid, electric mobility, and renewable energies frameworks.

MARÍA PAZ COMECH received the degree in industrial engineering, in 2003, and the Ph.D. degree in electrical engineering from the University of Zaragoza, in April 2008. Her Ph.D. dissertation was titled, "Analysis and Testing of Wind Systems in the Event of Voltage Dips."

Currently, she develops her research career within the Group T41_20R: Intelligent Optimization of the Generation and Integration of Renewable Sources (SMART-e), CIRCE Mixed University Research Institute, of which she is the third Deputy Director. Her research interests include the analysis and development of new smart grid structures and new grid control and automation algorithms, the study of the integration of renewable generation and distributed resources and their possible impact on quality, network efficiency and security; modeling, simulation and the analysis of electrical systems in PSCAD, PSS/E, and DIgSILENT PowerFactory, and the validation of computer models of systems. She has participated as a researcher in more than 120 R + D + i contracts with private financing, seven national projects and three belonging to the FP7 Framework program.

NOEMÍ GALÁN-HERNÁNDEZ received the B.S. degree in industrial engineering with specialization in industrial electrics from the Polytechnical University of La Almunia, Zaragoza, Spain, and the M.S. degree in renewable energies from the CIRCE Research Centre, CIRCE Mixed Research Institute, University of Zaragoza, Zaragoza.

Since 2014, she has been a Research Fellow and a Research and Development Project Manager with the Research Centre for Energy Resources and Consumption (CIRCE), Zaragoza, in both EU-funded and national-funded projects in the fields of renewable energies integration and smart grid, such as PARITY, SYNERGY, or in private-funded technology transfer projects, such as inter-area oscillation damping. She is currently a Line Manager of the Electric Networks Operation and Planning Team, Research Centre for Energy Resources and Consumption (CIRCE), Zaragoza. Since 2018, she has been an Adjunct Lecturer in integration of renewable energies and DIgSILENT PowerFactory in several M.S. courses provided by CIRCE), EUREC, and the University of Zaragoza. Her research interests include integration, optimization and forecasting algorithms in the smart-grid, renewable energies, and HVDC-VSC frameworks.